# STM Study of Copper Growth on ZnO(0001)−Zn and ZnO(000$\bar{1}$)−O Surfaces

**Lynn Vogel Koplitz,[†] Olga Dulub,[‡] and Ulrike Diebold*[,‡]**

*Department of Chemistry, Loyola University, New Orleans, Louisiana 70118, and Department of Physics, Tulane University, New Orleans, Louisiana 70118*

*Received: May 5, 2003; In Final Form: July 9, 2003*

The room-temperature growth of Cu on the polar (0001)-Zn and (000$\bar{1}$)-O surfaces of zinc oxide has been studied with scanning tunneling microscopy (STM). Copper grows on the (0001)-Zn surface as three-dimensional clusters even at low coverages (0.05−0.25 monolayers (ML)); two-dimensional (2D) islands are only observed at very low coverages (0.001−0.05 ML). The average size of the 3D clusters increases with coverage, and their density increases slowly. Surface roughness and sputter damage change the growth mode to more 2D-like. The Cu clusters are well-separated and exhibit a well-defined hexagonal shape. Equilibrium crystal shape analysis yields an apparent work of adhesion of $3.4 \pm 0.1$ J/m$^2$ for the largest clusters. On the (000$\bar{1}$)-O surface, formation of two-dimensional Cu clusters was observed at coverages of less than 0.1 ML.

## 1. Introduction

The growth of Cu on ZnO surfaces is particularly interesting due to the importance of Cu/ZnO catalysts in the low-temperature synthesis of methanol,[1−4] the production of hydrogen by steam reforming[5,6] or decomposition of methanol,[7] and the water-gas shift reaction for CO removal from reformed fuels to enable their use in fuel cells.[8,9] Similar catalysts have also been used in the dehydrogenation of cyclohexanol to cyclohexanone,[10] an important reaction in manufacturing caprolactam, which is used to make nylon-6.

There is agreement that a ZnO support leads to highly dispersed Cu catalyst,[3] but the nature and location of the active sites are still subject to a heated debate. Questions include the electronic structure of the active Cu clusters, their morphology, the nature of the interaction of the Cu with ZnO substrate, and the exact role of the ZnO in the catalytic activity of Cu. The literature on studies of methanol synthesis catalysts is somewhat contradictory. Either metallic Cu atoms[11,12] or special sites (potassium atoms) in addition to Cu are credited as active centers.[13] As for the ZnO substrate, models range from inert ZnO merely increasing the dispersion of Cu[11] to Cu−ZnO surface alloy formation.[3,4,14] Yet another scenario has ZnO act as a reservoir of adsorbed hydrogen, which "spills over" onto metallic Cu surfaces and enhances the hydrogenation process.[15−17]

The real catalyst is a complex system, and many different processes are involved. To understand the mechanisms of these reactions, it is useful to study a model catalyst system with certain assumptions and simplifications using surface science techniques. For this reason, ZnO single-crystal surfaces have been the subject of extensive surface science studies.[18,19] The polar faces of ZnO are of particular interest because they were shown to be the active faces in hydrogenation reactions and hence in methanol production.[20,21] In a simple model of a catalyst, metal particles are dispersed on single-crystal surfaces. The growth of many different metals on oxide surfaces has been studied and summarized in extensive review articles.[18,22,23]

A variety of nonimaging techniques, such as the low energy ion scattering (LEIS), X-ray photoelectron spectroscopy (XPS), electron energy loss spectroscopy (EELS), Auger electron spectroscopy (AES), and others have been used in the previous studies of Cu absorption on the (10$\bar{1}$0),[24−26] (11$\bar{2}$0),[27] (0001)-Zn,[26,28−30] and (000$\bar{1}$)-O[26,31−35] surfaces of ZnO. However, the initial stage of Cu growth (up to a coverage of several monolayers) is still controversial. The Cu surface energy (∼1.9 J/m$^2$)[36] is about twice as large as the surface energy of the nonpolar ZnO surfaces (∼1 J/m$^2$).[37] Thus, in thermodynamic equilibrium, a Volmer−Weber (VW) growth is predicted (i.e., formation of 3D clusters). This is true in general for most metals deposited on oxide surfaces.[18,22,23] Most of the growth is performed at room temperature and at low deposition flux, so it is reasonable to expect the growth mode to follow thermodynamic guidelines, although kinetic effects may certainly play a role. However, experimental studies have yielded conflicting results. Didziulis et al.[26] found that the first monolayer of Cu wets the ZnO substrate. In more recent studies, Cu was reported to grow two-dimensionally only up to a certain "critical" coverage, beyond which three-dimensional clusters form.[18,28,30,31,35] Campbell et al.[18] proposed that this "pseudo-layer-by-layer" growth mode is due to kinetic limitations. Essentially, Cu atoms that land at the ZnO surface during the deposition process are attracted to the step edges of 2D islands, and Cu atoms landing on the 2D islands experience a small activation barrier for downstepping. The latter barrier increases as soon as a second layer of Cu starts to form (see ref 18 for a more detailed description). The features of this model are valid for any metal/oxide system and Cu growth on ZnO has become *the* model system for studying the initial 2D growth of metal overlayers on metal oxide surfaces.[35] Experiments show that the critical coverage depends on sample orientation and preparation. For example, for the O-terminated ZnO surface, it is twice as high as for the Zn-terminated face. This observation could be attributed to different densities of nucleation sites, such as defects, on the surfaces, to a different strength of Cu bonding to the two faces, or both.

Scanning tunneling microscopy (STM) is a direct imaging technique and clearly suited best to study the nucleation behavior

* To whom correspondence should be addressed. Tel.: 504-862-8279. Fax: 504-862-8702. E-mail: diebold@tulane.edu.
[†] Loyola University.
[‡] Tulane University.

10.1021/jp0352175 CCC: $25.00 
Published on Web 08/28/2003

of metals on model catalysts. Despite the importance of the Cu/ZnO system in catalysis and its status as a model system for metal/oxide growth in surface science, very limited STM data exist to support the current view of Cu/ZnO, or to reconcile some of the conflicting evidence. A previous STM study of Cu growth on ZnO($10\bar{1}0$) by our group unraveled the influence of step edges on cluster nucleation and the influence of surface contamination on the critical coverage for the 2D−3D growth mode transition.[24]

In this paper, the morphology of Cu films, deposited on polar (0001)-Zn and ($000\bar{1}$)-O surfaces of ZnO at room temperature, is investigated with STM for the first time. Three-dimensional cluster-growth mode is observed on the (0001)-Zn surface at much lower coverages than reported in previous studies. A strong dependence of Cu growth on surface defects is observed. An analysis of the shape of the Cu clusters allows an estimate of the apparent work of adhesion of Cu/ZnO as a function of particle size. This quantity is key for understanding the strength of the metal-to-oxide bonding and relevant for predicting a variety of properties such as particle shape, chemisorption of the particles, and resistance to re-dispersion and sintering.[38] The growth mode on the ($000\bar{1}$)-O surface is different from the Zn-terminated face; on the O-terminated surface, Cu grows preferentially in 2D clusters.

## 2. Experimental Section

The experiments were carried out in an ultrahigh vacuum (UHV) chamber with a base pressure of $\sim 2 \times 10^{-10}$ mbar. The chamber is equipped with the experimental facilities for low-energy $He^+$ ion scattering spectroscopy (ISS), low-energy electron diffraction (LEED), and STM.

ZnO single crystals, grown by the hydrothermal method, were obtained from the MTI Corporation. Samples, 10 mm × 5 mm × 0.5 mm in size, were cut, polished, and oriented to within 0.5° of the *c*-axis. The polarity of the crystals was determined ex-situ by their chemical etching behavior in HCl solution (the oxygen face of ZnO etches more rapidly than the Zn face[39]), and in-situ by ISS Zn/O peak ratios. Samples were cleaned by cycles of $Ar^+$ ion bombardment (1 keV, 0.7 $\mu$A) at room temperature and annealing up to 750 °C for 5 to 20 min until no contamination could be detected with ISS, and a sharp (1 × 1) LEED pattern was observed. Samples were heated radiatively and their temperature was monitored by a thermocouple spot-welded close to the sample holder.

Copper was vapor-deposited onto the clean sample at room temperature (RT) using a homemade evaporation source. A piece of Cu wire (99.999% purity) was placed in a 3 mm × 3 mm Ta basket spot-welded to a tungsten wire. Both ends of the wire were connected to electrodes, and the basket temperature was monitored with a thermocouple. A current of 6.5 A was used to heat the basket to the Cu evaporation temperature of 1100 °C. The Cu source was thoroughly outgassed prior to evaporation. The sample was placed approximately 10 cm away from the evaporator, and the substrate temperature was always below 40 °C during Cu evaporation. The pressure during Cu deposition remained below $5 \times 10^{-10}$ mbar in the UHV chamber. A deposition rate of 0.0013 Å × $sec^{-1}$ was used in all experiments. The deposition rate was calibrated by a quartz crystal microbalance before growth and checked with STM by a statistical analysis of cluster densities and heights. The height of the clusters was measured from the cluster's profile cross section from the top of each cluster to its base. The width of the clusters was measured at mid-height level, averaging over two cross-sections. The aspect ratio of Cu clusters with well-defined shapes was used to calculate the work of adhesion (see section 4.2) and was determined somewhat differently in accord with a procedure reported previously.[40] In this case, Cu clusters with well-defined flat top faces were used and the width was measured between the two points on the line profile where the line starts to bend down. The concentration of deposited Cu is given in monolayer equivalent (ML), which corresponds to a Cu(111) packing density of $1.7 \times 10^{15}$ Cu atoms per $cm^2$. The expected thickness of one layer of Cu(111) is 2.2 Å.

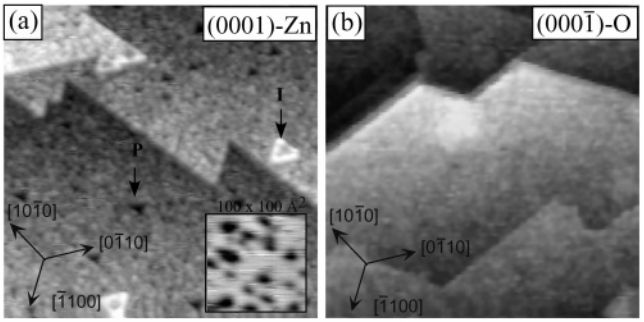


**Figure 1.** STM images (500 × 500 Å$^2$) of polar surfaces of ZnO annealed to 750 °C for 15 min: (a) (0001)-Zn; (b) ($000\bar{1}$)-O.

The STM experiments were carried out using an Omicron UHV-STM-1 at room temperature. All STM data were recorded in constant current mode at a positive sample bias of 1.5−2.5 V (negative bias voltage generally resulted in unstable tunneling) and with a feedback current of 0.8−1.8 nA. Electrochemically etched W tips, cleaned by argon sputtering and by applying voltage pulses during operation, were used in the STM. STM results are presented as top-view images with darker colors corresponding to lower apparent heights.

## 3. Results

**3.1. Clean ZnO(0001)−Zn and ($000\bar{1}$)−O Surfaces.** Before describing copper growth on ZnO(0001)-Zn and ZnO($000\bar{1}$)-O, a short description of the clean surfaces as well as their appearance in STM is in order. ZnO has a hexagonal crystal structure with the main lattice parameters $a = 3.25$ Å and $b = 5.206$ Å.[41] Its structure can be described schematically as a number of alternating planes stacked along the *c*-axis and composed of 4-fold-coordinated $O^{2-}$ and $Zn^{2+}$ ions. A ZnO crystal does not have a center of symmetry (no symmetry elements perpendicular to the *c*-axis), resulting in two polar surfaces on opposite sides, each terminated by one type of ions only. From an electrostatic point of view, polar surfaces should not be stable unless charge rearrangement (charge reduction by a factor of ~1/4 in the case of ZnO) on the topmost surface layers takes place. This can occur through three mechanisms: (1) charge transfer from the O to Zn surface and creation of surface states; (2) positively (negatively) charged impurity atoms on the O (Zn) surfaces; (3) removal of surface atoms. Each of these compensation mechanisms is expected to affect the growth of metal overlayers in a very different way.

The morphology of the polar surfaces of ZnO after preparation in UHV was discussed in detail in ref 42. STM images of (0001)-Zn and ($000\bar{1}$)-O surfaces prepared by sputtering and then annealing for 15 min at 750 °C are shown in Figure 1. Both polar surfaces are unreconstructed and exhibit a (1 × 1) LEED pattern with a 6-fold symmetry. (Refs 42 and 43 explain why a 6-fold symmetry is observed, instead of the 3-fold symmetry expected from the hexagonal structure of ZnO.)

The ZnO(0001)-Zn surface presented in Figure 1a exhibits large terraces, ranging in width from 100 to 250 nm. The terraces have a triangular shape and are separated by single-layer high (~2.6 Å) steps. Many single-step-deep triangular pits and single-

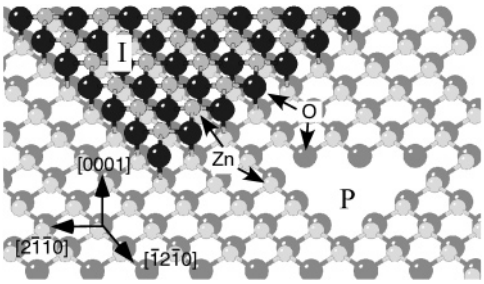


**Figure 2.** Atomic model of the bulk terminated (0001)-Zn surface with a single layer triangular terrace and pit.

step-high islands (labeled P and I in Figure 1a, respectively, are present on the terraces. Small islands have special shapes.[44] The size of the terraces and triangular pits depends critically on the annealing temperature. Annealing at 400−600 °C induces small terraces and a high density of triangular pits. Terraces grow wider and triangular pits become smaller after annealing at higher temperature (∼750 °C). (However, even on the well-annealed surface, some areas were found to be highly stepped (see the area in the left corner in Figure 7a, discussed below) with terrace widths of 20−160 Å, which is probably an artifact of the surface polishing). In ref 44 we have shown that the small pits contribute to the stabilization of ZnO(0001)-Zn and thus are intrinsic to this surface. All step edges on the (0001)-Zn surface are O-terminated, thus creating the Zn-deficient surface, consistent with mechanism (3) mentioned above (see the model in Figure 2). This is confirmed by density functional theory (DFT) calculations that show that surfaces with triangular holes are stable over a wide range of $O_2$ and $H_2$ chemical potentials.[44] For the preparation conditions employed in this study, triangular features clearly have the lower surface energy. It is important to keep the resulting "rugged" surfaces in mind, as surface defects often have a strong effect on growth and nucleation of overlayers.

A distinctly different surface morphology was consistently observed on the (000$\bar{1}$)-O surface. Figure 1b shows hexagonal terraces, ∼200−400 Å wide. The terraces are smooth and do not have any small pits or islands. Occasionally, big (∼200 Å wide) hexagonal holes are observed on the surface. The terraces are mainly terminated by double-layer-high (∼5.2 Å) stoichiometric steps running at an angle of 120° with respect to each other. While O-terminated step edges (i.e., Zn deficiency) provide the necessary electrostatic stabilization on the (0001)-Zn surface, a different mechanism must be at work on the (000$\bar{1}$)-O surface. Several charge-compensation mechanisms for the (000$\bar{1}$)-O surface were proposed, but the matter is still quite controversial. Wander et al. performed ab initio calculations on ZnO that predicted two-dimensional metallic layers on both polar surfaces occurring through charge transfer between the O- and Zn−terminated faces (mechanism (1)).[45] However, the expected two-dimensional metallic states have not been observed experimentally.[46,47] Dissociative adsorption of water and $H^+$ and $OH^-$ groups were also considered.[45,48−50] These recent results suggest that it is unlikely that a clean, defect-free (000$\bar{1}$)-O surface can be observed experimentally.[50]

**3.2. Cu growth on ZnO(0001)−Zn Surface.** Figure 3a shows an STM image of 0.005 ML of Cu deposited on the (0001)-Zn surface at room temperature. Copper clusters ∼3 Å high and 10−18 Å wide are formed on the surface, with no apparent preferential nucleation sites. As the inset of Figure 3a shows, Cu clusters are round in shape. The diameter of the clusters cannot be measured accurately due to convolution by the tip shape. However, the height of the clusters can be

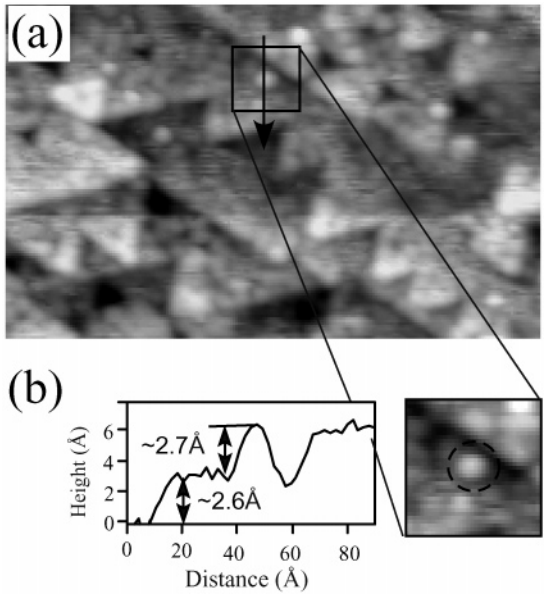


**Figure 3.** (a) STM image (400 × 250 Å$^2$) of 0.005 ML of Cu deposited on (0001)-Zn. (b) Line profile of a 2D cluster on the surface.

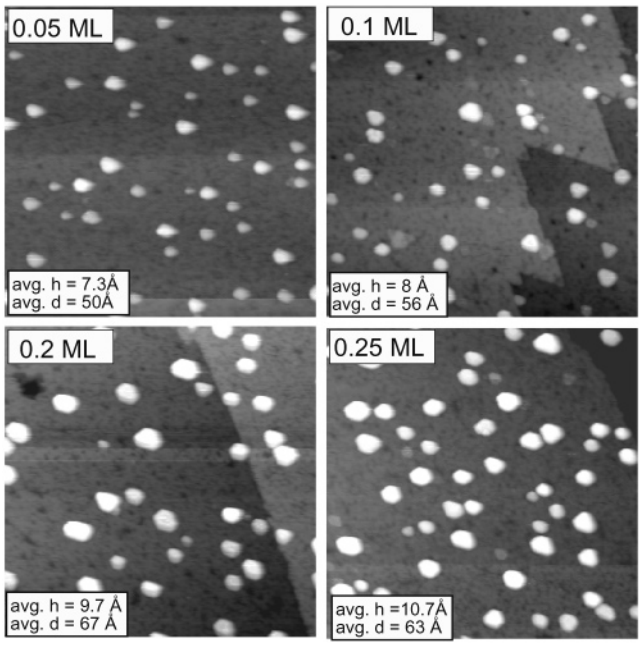


**Figure 4.** STM images (1000 × 1000 Å$^2$) of the polar (0001)-Zn surface after deposition of 0.05, 0.1, 0.2, and 0.25 ML of Cu, as well as average sizes of Cu clusters (averaged over 4 images for each coverage).

determined by comparison with the height of the single-layer steps, as shown in the line profile of Figure 3b. Because this is a line profile of the smallest clusters observed, we assume that it corresponds to Cu clusters one monolayer high, and assign ∼2.7 Å as the apparent height of a Cu monolayer on the ZnO(0001)-Zn surface.

Further deposition of Cu leads to formation of large, well-separated and uniformly distributed Cu clusters. Figure 4 shows STM images of Cu coverages varying from 0.05 to 0.25 ML, as well as the height and diameter of Cu clusters (averaged over at least 40 clusters for each coverage). The average cluster size increases with increasing Cu coverage, whereas the density of clusters remains almost constant. Although at very small coverages (0.005−0.01 ML) Cu clusters are exclusively two-dimensional (top graph of Figure 5), the height-to-width ratio

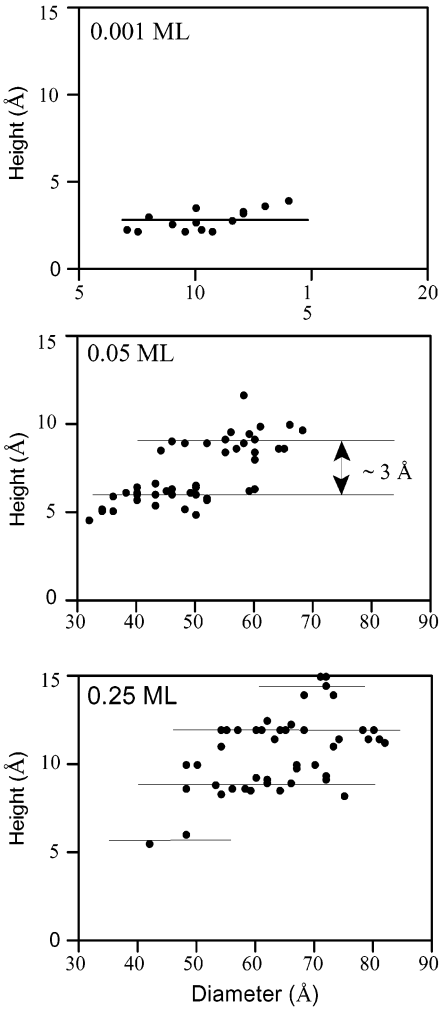


**Figure 5.** Cu island heights as a function of coverage for Cu on ZnO(0001)-Zn, deposited at RT.

of 3D clusters grows rapidly with further deposition. As shown in Figure 5, at 0.05 ML most of the clusters are either two or three monolayers high. At 0.25 ML, one can observe cluster heights ranging from two to five monolayers, but hardly any 2D clusters.

An STM image after deposition of 0.25 ML of Cu and line profiles of two clusters are shown in Figure 6. The hexagonal shape of large clusters becomes visible at high coverages, as indicated by the outline of the cluster in the inset of Figure 6a. Occasional 2D clusters are still present on the surface. The line profile in Figure 6b shows both a 2D cluster, ~2.7 Å high, and a 3D cluster, ~15 Å high.

To investigate the influence of the residual gas on the Cu growth mode on the (000$\bar{1}$)-Zn surface, which showed a strong effect in the Cu/ZnO(10$\bar{1}$0) system, a clean surface was kept at a pressure of $5 \times 10^{-10}$ mbar for 3 h before Cu deposition. The prolonged exposure to this untypically high pressure did not influence the growth behavior of Cu on this surface, in contrast to observations for the (10$\bar{1}$0) surface.[24] The character of the Cu overlayer does depend on the surface roughness, however. Rougher surfaces may result from lower annealing temperature, or can be a consequence of imperfect crystal polishing. In our case, even well-annealed surfaces occasionally exhibit rough, highly stepped areas (Figure 7a). In such areas, the clusters appear smaller in diameter and higher in concentration. The density of 2D clusters also increases significantly compared to the neighboring smooth large terraces (Figure 7b).

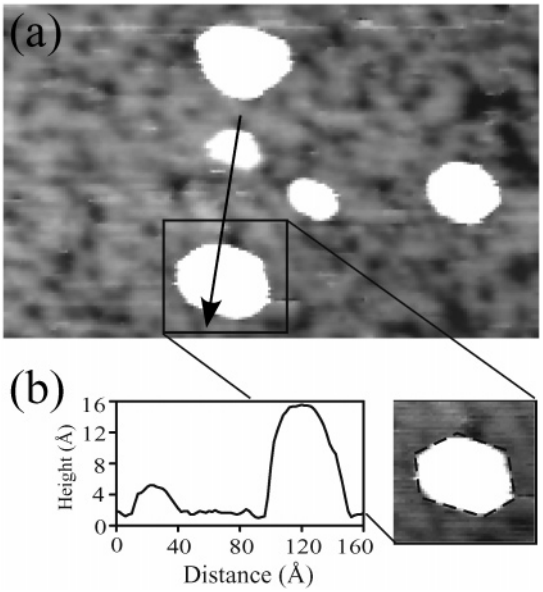


**Figure 6.** (a) STM image (400 × 250 Å$^2$) of 0.25 ML of Cu deposited on (0001)-Zn. (b) Line profile of typical 3D and 2D clusters on the surface.

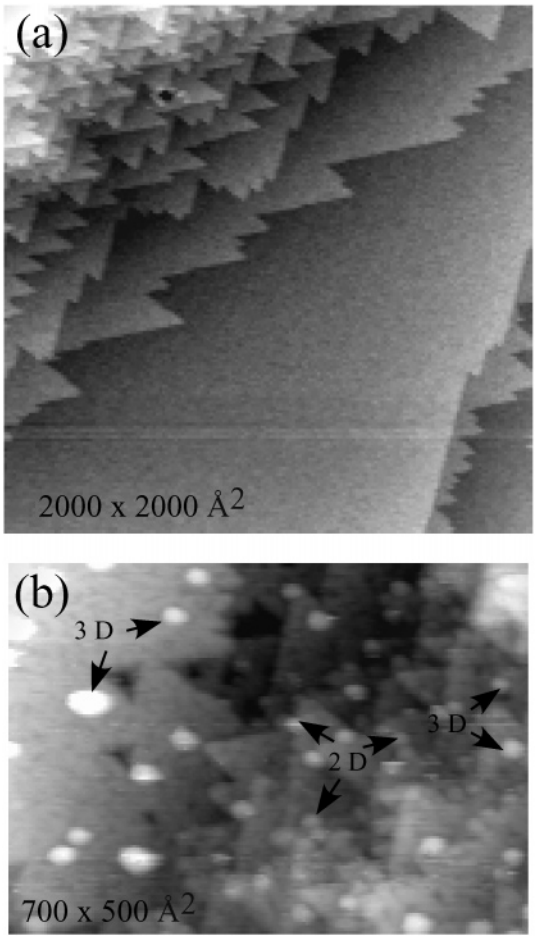


**Figure 7.** STM images of ZnO(0001)-Zn surface (a) before Cu deposition and (b) after deposition of 0.025 ML of Cu.

When an annealed surface was bombarded with Ar ions (exposure to 1 keV $Ar^+$ for 3 min at a current of 0.6 $\mu$A) before copper deposition, a drastic increase in the density of 2D Cu clusters was observed. Such a slightly sputtered surface is expected to have a different type of defects, as well as a higher defect density than a well-annealed surface.

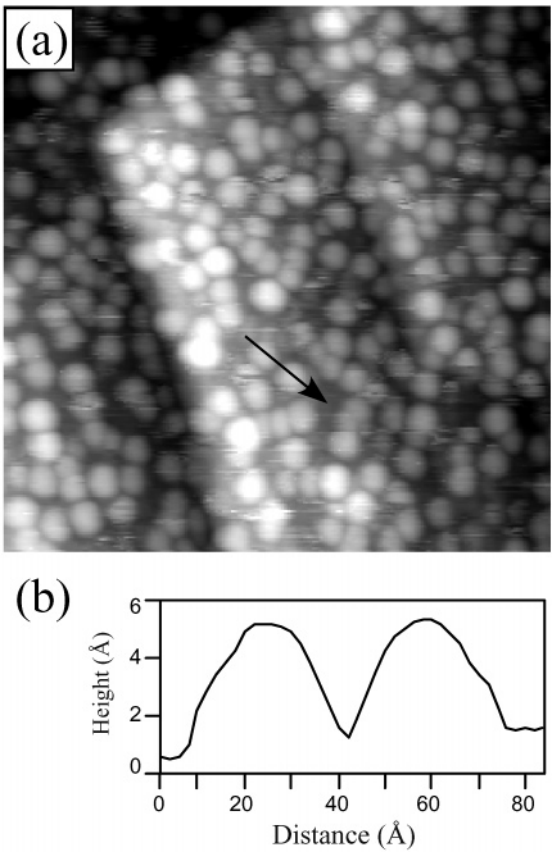


**Figure 8.** (a) STM images (500 × 500 Å$^2$) of ~0.1 ML of Cu on the (000$\bar{1}$)-O surface. (b) Line profile of two typical clusters.

**3.3. Cu growth on ZnO (000$\bar{1}$)-O Surface.** An STM image of the (000$\bar{1}$)-O surface after deposition of ~0.1 ML of Cu is shown in Figure 8a. Even at low coverages, a high density of clusters is uniformly distributed over the surface. The shape of the clusters is not well-defined, and some of the adjacent clusters coalesce. The line profile of two typical clusters is shown in Figure 8b. The smallest clusters observed are ~4.3 Å high, which could correspond to a 2D growth mode, given the ambiguity in measuring cluster heights grown on electronically dissimilar materials. Clusters appear to be rounded in shape and are ~15−25 Å in diameter. Clusters are measured to cover more than 10% of the surface (at only 0.1 ML coverage), which indicates that the cluster diameters are overestimated due to the tip convolution effect.

Investigating Cu growth on this surface posed significant technical difficulties. In general, more cleaning cycles are required to clean the (000$\bar{1}$)-O surface than the (0001)-Zn face, and a very small Ca peak is almost always detected in ISS. It was hard to consistently prepare microscopically flat surfaces with a well-defined terrace structure. Sometimes the STM tip would not approach, indicating that the surface possibly becomes more insulating. During the STM study, strong tip−surface interaction very often led to "double tip" features on the surface. No systematic study of Cu deposition as a function of coverage could be performed, but for the coverages studied (0.01−0.1 ML), a 2D growth mode was dominant.

## 4. Discussion

**4.1. Growth Mode and Factors Affecting the Growth.** In light of earlier results reported for the Cu/ZnO system, two of our observations are remarkable. First, on the annealed (0001)-Zn surface, no preferential nucleation on the surface defects that are intrinsic to this surface (i.e., the pits and step edges of small islands) was observed in our study. Intuitively, one would expect such defect sites to act as principal nucleation centers. Second, the 2D−3D transition in the growth mode was observed to occur at a coverage that is at least an order of magnitude lower than the critical value of 0.33 ML that was observed in earlier studies[28] utilizing area-averaging techniques. The results displayed in Figure 7 may help to clarify both issues. Figure 7 shows STM images of the (0001)-Zn surface before and after deposition of 0.025 ML of Cu. The Cu clusters on the wide terrace in the left half of Figure 7b are large and 3-dimensional, while on the right side, where the surface is rough with many small terraces, small, mostly 2-dimensional clusters are observed. This can be explained by invoking kinetic barriers,[51] where Cu adatoms that diffuse along the surface are effectively repelled from step edges. This prevents Cu atoms from stepping down to the lower terrace and from stepping up onto the upper terrace. Provided that the effective diffusion length of Cu is larger than the width of the terrace, the Cu atoms become confined to the terraces they initially land on. Consequently, the size of the clusters will scale with the size of the terrace they reside on. We do not have any quantitative information on the height of the repulsive barriers at the step edges, but it is interesting to note that all the step edges of ZnO(0001)-Zn are oxygen terminated (see Figure 2). If one assumes that Cu interacts more strongly with Zn than with O surface atoms (see below), this kinetic barrier could be quite sizable.

Figure 7b shows that the size of the clusters is proportional to the size of the underlying terrace, supporting this idea. The surface on the right-hand side of Figure 7b exhibits many narrow terraces. Since the number of Cu atoms a terrace collects is proportional to its area, and the collected atoms are prohibited from moving between the terraces, there are not enough Cu atoms to initiate 3D growth on these terraces even at relatively high total Cu coverages. Correspondingly, mostly 2D clusters are observed on the rough patch of the surface. On the other hand, there is enough Cu to initiate 3D growth at the neighboring wide terrace. Interestingly, the presence of high repulsive barriers also explains why the numerous small pits, present at the wide terraces of well-annealed samples (see Figure 1a) do *not* act as nucleation sites; the sides of these pits are also O-terminated and Cu atoms landing on the terrace cannot step down into these small pits. If, however, other types of defects are induced on wide terraces (for example, by sputtering), the diffusion of Cu is inhibited, which leads to the nucleation of a larger number of smaller clusters.

These facts clearly indicate that the critical coverage (for the 2D to 3D transition) can depend strongly upon the roughness and extrinsic defects of the surface. A difference in surface roughness could partially be responsible for the discrepancy in the data on critical coverage in the literature. The role of the kinetic barriers in driving the size of the clusters and the distribution of nucleation sites was also observed on the nonpolar (10$\bar{1}$0) surface of ZnO.[24] In that case, the results were interpreted by invoking a repulsive barrier for down-stepping (the so-called Ehrlich-Schwoebel barrier).[51] The major difference between Cu growth on the (10$\bar{1}$0) and (0001)-Zn surfaces is that on the former surface, Cu adatoms are constrained to move along the dimmer rows and are driven into the step edges from the lower terrace (which are terminated with both kind of atoms, O and Zn). The Zn-terminated polar surface has a 3-fold symmetry without any preferred diffusion paths for Cu atoms.

A very different growth mode was observed for the O-terminated surface, where the STM showed 2D clusters

randomly distributed across the surface. As pointed out in Section 3.1, the mechanism that stabilizes the $(1 \times 1)$-terminated surface is not understood. Mechanism (3) (nonstoichimetry) can probably be excluded, but the other two possibilities (i.e., (1) a different surface charge or (2) impurity atoms, particularly hydrogen) will affect the kinetics and dynamics of copper growth on this surface. Without a reliable answer to the question of how the surface reacts to the electrostatic instability of a $(1 \times 1)$-terminated configuration, we can only speculate on the reason for the apparent 2D growth of Cu on ZnO$(000\bar{1})$-O. A different surface charge, in particular surface oxygen atoms that are not as ionic as in the bulk, could lead to strong bonding by substantial charge transfer between the copper atoms and the surface. Impurity atoms could influence the Cu growth mode by either lowering Cu adatom mobility or by providing strong adsorption sites for Cu atoms. This implies that both the kinetics and the thermodynamics of the growth would be affected, as the latter would lower the interfacial energy and improve wetting. Similar effects of contaminants increasing the density of Cu clusters significantly were also observed in the study of Cu growth on the $(10\bar{1}0)$ surface of ZnO.[24] Some STM images of clean ZnO$(000\bar{1})$-O exhibit bright spots attributed to the subsurface impurity defects. These defects can also potentially act as preferential nucleation sites for Cu.

**4.2. Work of Adhesion of Cu Clusters on ZnO(0001)−Zn.** The three-dimensional growth of Cu on the (0001)-Zn surface suggests stronger Cu−Cu than Cu−ZnO interaction, and a high mobility of Cu adatoms on the surface. At low coverages, 3D clusters appear to be rounded in shape, but as they grow larger with the increase of coverage, they start to exhibit a well-defined hexagonal shape. While some of this evolution of cluster shape could be simply attributed to the difficulty of measuring small islands with STM, the large lattice mismatch (21%) between Cu(111) and ZnO will also play a role. Cu clusters are expected to be strained, especially at lower coverages. Previous TPD results of CO adsorption on Cu film on ZnO$(000\bar{1})$-O indicated formation of the Cu(110) plane at small coverages while the transition to Cu(111)-like sites occurred at higher coverages (>55%) and after annealing.[35]

To understand the nature of metal/metal oxide surface interactions, it is desirable to determine the energy of adhesion, also called the work of adhesion, $W_{adh}$, for these systems. This quantity is defined as the amount of energy per unit area required to pull metal clusters apart from the oxide substrate surface, assuming a simple system with no strain in the clusters and no diffusion between the metal clusters and oxide substrate. Besenbacher's group introduced a technique whereby $W_{adh}$ can be derived from STM measurements.[40,52] These investigators analyzed the dimensions of metal clusters from STM images using a relationship they developed between cluster height/width ratios and metal surface free energies based on earlier work by Kaischew[53] and Winterbottom.[54] We used this approach to find $W_{adh}$ for Cu/ZnO(0001)-Zn from our STM images as described below.

Worren et al.[40] use the Wulff-Kaischew theorem,[55] the Dupré equation[56] and geometric relationships for an appropriate Wulff polyhedron[57] to develop a function relating the work of adhesion for a face-centered-cubic metal cluster to the surface energies of its low-index planes, $\gamma_{hkl}$, and measured ratios of cluster height, $H$, to the width of the top facet, L.

$$W_{adh} = 2\gamma_{111} - H/L\,(-3/\sqrt{2}\gamma_{111} + \sqrt{3}\gamma_{110} + \sqrt{3}/\sqrt{2}\gamma_{100}) \quad (1)$$

This approach will be valid for Cu clusters on ZnO if they achieve an equilibrium shape (Wulff polyhedron) containing (110) facets. As part of their work on $Cu/Al_2O_3/NiAl(110)$, Worren et al.[40] calculated that Cu clusters with a top facet width greater than ~40 Å would have (110) side facets. In the case of a face-centered-cubic crystal resting on a (111) facet with a parallel (111) plane facing up toward the STM tip, a Cu cluster shaped as a Wulff polyedron will appear to be hexagonal in an STM image.[23] Although we were unable to achieve atomic resolution on the top facets of the Cu clusters, the shape of the clusters strongly suggests that they are (111)-oriented (Figure 6). This orientation is in agreement with HRTEM observations for Cu/ZnO by Hansen et al.[58] and also reported by Campbell.[18] In addition, Worren et al.[40] confirmed the top facet of Cu islands on $Al_2O_3$/NiAl to be the (111) surface.

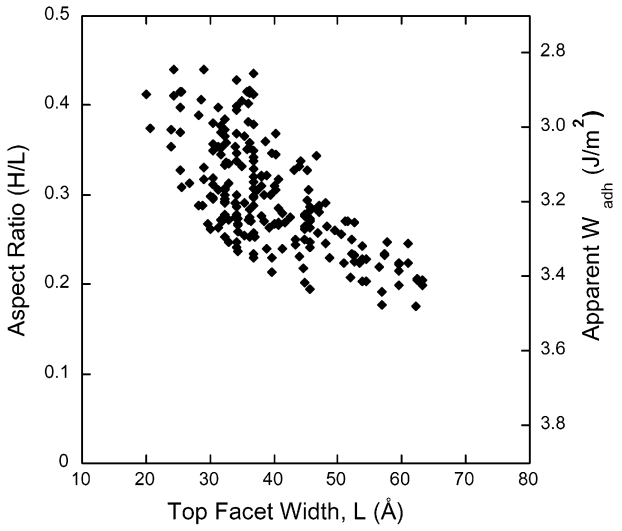


**Figure 9.** Measured height-to-width ratio for well-separated hexagonal Cu clusters on the ZnO(0001)-Zn surface. Right axis: The apparent work of adhesion, derived from the $H/L$ values using eq 1 and the surface free energies from ref 36. (Note: $W_{adh}$ values shown only apply to clusters with $L \geq 4$ nm.)

Figure 9 shows the height-to-width aspect ratio, $H/L$, plotted versus the top facet width, $L$, for 73 islands (219 $H/L$ values) from 15 different STM images with Cu coverages ranging from about 0.05 to 0.3 ML. All islands were isolated and appeared to be hexagonal though not generally symmetric (that is, the side length ratio was not usually 1) with flat line scans across the top facet. Following Besenbacher, Stensgaard, and co-workers,[40,52] we base our calculation of $W_{adh}$ on the lowest $H/L$ values (observed for the widest clusters), or about $0.21 \pm 0.04$, where the equilibrium shape is most likely to be fully developed.

Deriving absolute values for $W_{adh}$ from eq 1 is complicated by the fact that literature values for surface energies vary substantially.[36,59,60] Mattsen and Jennison[61] recently pointed out the difficulties in obtaining accurate surface energies with DFT. Due to a fortuitous cancellation of errors, numbers based on the local density approximation (LDA) are more reliable than numbers based on the generally more accurate generalized gradient approximation (GGA). For this reason, and to enable comparison with previous experiments, we use the values given by Vitos et al.[36] (i.e., $\gamma_{111} = 1.95$, $\gamma_{110} = 2.24$, and $\gamma_{100} = 2.17$ J/m$^2$). From eq 1 above, $W_{adh}$ converges to a value of $3.4 \pm 0.1$ J/m$^2$ for high coverages (see Figure 8). (If we use values derived from a tight-binding calculation,[59] then $W_{adh} = 3.0 \pm 0.1$ J/m$^2$, and averaged with results above this gives $3.2 \pm 0.3$ J/m$^2$). Only a few literature reports of quantitative measurements of $W_{adh}$ on well-characterized single crystalline surfaces are available for comparison. The $W_{adh}$ for both $Pd/Al_2O_3/NiAl(110)$ and Cu/

$Al_2O_3$/NiAl(110) was reported to be 2.8 ± 0.2 J/m$^2$.[40,52] Campbell and co-workers[62] have derived adhesion energies from microcalorimetry measurements for systems including Pb, Ag, and Cu on MgO(100)/Mo(100). Their reported values are 0.77 ± 0.20, 0.30 ± 0.30, and 1.92 ± 0.60 J/m$^2$, respectively.

Perhaps most relevant to this study is the recent work by Hansen and co-workers[58] where they used HRTEM to investigate dynamic shape changes of Cu nanocrystals on ZnO surfaces under different gaseous environments. Our results should be compared to the most reducing conditions used in ref 58, where flat, (111)-terminated Cu clusters were observed with a $W_{adh}$ of 3.00 ± 0.10 J/m$^2$ (They report $W_{adh}$ as a unitless 1.54 ± 0.05, because it is normalized to an unspecified value of $\gamma_{111,vac}$. Multiplication of this $W_{adh}$ by the appropriate surface energy $\gamma_{111}$ = 1.95 J/m$^2$ used for the rest of our comparisons[36] gives 3.00 ± 0.10 J/m$^2$). This number lies well within the range of $W_{adh}$ values displayed in Figure 9. An even more appropriate comparison can be made if we note that clusters with a size between 3 and 6 nm were analyzed in ref 58. Because eq 1 is strictly valid only for clusters that have developed (110) side facets, and as detailed in ref 57, a modified version of eq 1 (with only the $\sqrt{3}/\sqrt{2}\ \gamma_{100}$ term inside the parentheses) applies to clusters with a size of less than 4 nm, two different relationships must be used with our data set to calculate an average $W_{adh}$ spanning the same range of cluster sizes analyzed in ref 58. Using the modified equation for smaller clusters with $3 \le L < 4$ nm and eq 1, where $L \ge 4$ nm gives an average $W_{adh}$ of 3.1 ± 0.2 J/m$^2$ for comparable clusters in our experiment. It is quite encouraging to find such close agreement between results from UHV surface science studies and the catalytic literature.

It is not unexpected that the value for Cu/ZnO is substantially higher than $W_{adh}$ found for Cu on $Al_2O_3$ and MgO. The ZnO(0001) surface is terminated with a layer of Zn atoms, hence a metal-to-metal bond is established at the interface. This is in contrast to the mixed cation/anion surfaces on MgO(001) and $Al_2O_3$(0001), used in the experiments quoted above. Bogicevic and Jennison[63] analyzed the nature of the bonding in the Pd/$Al_2O_3$ system and found that it was due to polarization (i.e., no significant charge transfer takes place at the metal/metal oxide interface). From calorimetry measurements, Campbell and Starr[62] concluded that the dominant interaction is the one between the metal overlayer with the Mg atoms of the substrate. A surface termination with metal atoms, as is the case in this experiment, will pose a situation with a possibly much stronger bonding interaction as compared to the other oxides investigated. In addition, zinc and copper are known to form stable alloys.[64] While we do not observe any evidence that alloy formation occurs at the interface between the Zn and the Cu clusters at room temperature, it can be taken as an indication that bonding between these two metals is quite favorable, leading to the relatively high $W_{adh}$ value.

As can be seen from Figure 9, smaller islands tend to show a higher aspect ratio with $H/L$ decreasing from near 0.4 at $L \sim$ 20 Å to about 0.2 at $L$ close to 65 Å. A similar trend was observed for Cu/$Al_2O_3$/NiAl(110), where the highest measured $H/L$ ratio was about 0.8 at $L \sim$ 19 Å and decreased to about 0.4 at $L \sim$60 Å.[40] Højrup Hansen et al.[52] also saw this trend in the Pd/$Al_2O_3$/NiAl(110) system where $H/L$ was about 0.35 for the smallest clusters ($L \sim$ 20−30 Å) then decreased to ∼0.18 for islands with $L >$ 55 Å. In both cases, the authors interpreted the leveling out of the ratios as an indication that equilibrium shapes were being achieved for the wider clusters such that adhesion energy could be based most appropriately on these stabilized H/L values. It is curious to note, however, that in all three cases, the stabilized aspect ratio is about half the ratio observed for the smallest hexagonal islands. This behavior suggests a consistently lower $W_{adh}$ for smaller clusters, or indicates some additional energy contribution of about the same magnitude as $W_{adh}$, in all three cases.

It is possible that strain, or plastic deformation, of the Cu lattice near the interface plays a major role. Straining a cluster costs energy and effectively decreases the energy gained by the binding of the cluster to the substrate. Giraou et al.[65,66] report direct observation of dilation of the first three layers in the lattice of Pd clusters on MgO(001), where the lattice misfit is 8%. Consequently, these investigators report what they call an "apparent adhesion energy" of ∼0.91 J/m$^2$ determined from HRTEM measurements of the dimensions of Pd clusters on MgO(001) with subsequent analysis using the Wulff-Kaischew relationship. (We use the same, more cautious, assignment of "apparent $W_{adh}$" for the energy on the right axis in Figure 8.) As mentioned previously, the lattice mismatch in our system is about 21%. While strain could contribute substantially to the total energy for small clusters where the first few layers account for a large fraction of the volume of the cluster, it would decrease in relative importance as the clusters grow larger. Also, smaller clusters will be more strained than bigger ones, where misfit dislocations can alleviate part of the strain.

One has to be careful not to over-interpret the apparent $W_{adh}$ values for small clusters. The energy was derived using two assumptions that might not necessarily be valid for clusters that are below a certain size. First, the equilibrium shape might not yet be fully developed for very small clusters (although great care was taken in our analysis to use only clusters with a well-defined shape). Second, strain might affect the values for the surface free energies, $\gamma$, that are used in our analysis. This effect could be addressed by a model that explicitly accounts for strain due to lattice mismatch as recently proposed by Müller and Kern.[67] Despite these caveats, it should be pointed out that the $H/L$ and corresponding apparent $W_{adh}$ results in Figure 9 represent the most comprehensive STM data set for nanoscopic clusters supported on a metal oxide surface to date.

## 5. Conclusions

We have presented the first STM study of Cu growth on polar ZnO surfaces. Contrary to previous results that were obtained with area-averaging techniques, STM clearly shows the formation of 3D Cu clusters, starting from very low coverages. The kinetic effects, previously proposed to govern the 2D to 3D transition, do not seem to play a major role for the Cu/ZnO(0001)-Zn system. Surface roughness and sputter-induced damage are important, however, as both skew the growth mode from clearly 3-D to more 2-D like. It was observed that the terrace size of the substrate affects the size and morphology of the Cu clusters and that small pits (which are intrinsic in the ZnO(0001)-Zn surface) do not act as dominant nucleation sites. These effects can be explained by invoking large repulsive barriers at the oxygen-terminated step edges on this surface. Consistent with previous results, Cu is observed to grow as 2D islands on the ZnO(000$\bar{1}$)-O surface. However, a better understanding of the nature of the clean O-terminated ZnO(0001)-O surface is needed to fully understand why this growth morphology develops.

The Cu clusters on the ZnO(0001)-Zn surface show well-developed facets. A quantitative analysis of the clusters' aspect ratio renders values for the apparent work of adhesion that converge to a value of 3.4 ± 0.1 J/m$^2$, in good quantitative

agreement with results from a Cu/ZnO catalyst. Because the interaction of Cu with a Zn-terminated surface is favorable, this value is high compared to that found for Cu on other metal oxides, which might partially explain why ZnO supports lead to highly dispersed Cu catalysts. The apparent $W_{adh}$ decreases with cluster size, probably due to strain effects in smaller clusters that lower the adhesion and/or the surface energy of the Cu clusters.

**Acknowledgment.** This work was supported by the National Science Foundation (Grant NSF-CHE-0109804) and NASA. We thank M. Batzill, I. Stensgaard, D.R. Jennison, and B. Meyer for their useful discussions.

## References and Notes

(1) Grunwaldt, J. D.; Molenbroek, A. M.; Topsœ, N. Y.; Topsœ, H.; Clausen, B. S. *J. Catal.* **2000**, *194*, 452.
(2) Ovesen, C. V.; Clausen, B. S.; Schiotz, J.; Stoltze, P.; Topsœ, H.; Nørskov, J. K. *J. Catal.* **1997**, *168*, 133.
(3) Fujitani, T.; Nakamura, J. *Appl. Catal., A* **2000**, *191*, 111.
(4) Choi, Y.; Futagami, K.; Fujitani, T.; Nakamura, J. *Appl. Catal., A* **2001**, *208*, 163.
(5) Loffler, D. G.; McDermott, S. D.; Renn, C. N. *J. Power Sour*. **2003**, *114*, 15.
(6) Günter, M. M.; Ressler, T.; Jentoft, R. E.; Bems, B. *J. Catal.* **2001**, 203, 133.
(7) Choi, Y.; Stenger, H. G. *Appl. Catal., B* **2002**, *38*, 259.
(8) Tanaka, Y.; Utaka, T.; Kikuchi, R.; Sasaki, K.; Eguchi, K. *Appl. Catal., A* **2003**, *242*, 287.
(9) Song, C. *Catal. Today* **2002**, *77*, 17.
(10) Lee, J.; Wang, C. C. *Hydrocarbon Process.* **1992**, *71*, 67.
(11) Chinchen, G. C.; Spencer, M. S.; Waugh, K. C.; Whan, D. A. *J. Chem. Soc. Faraday Trans. 1* **1987**, *83*, 2193.
(12) Pan, W. X.; Cao, R.; Roberts, D. L.; Griffin, G. L. *J. Catal*. **1998**, *114*, 440.
(13) Sheffer, G. R.; King, T. S. *J. Catal.* **1989**, *115*, 376.
(14) Harikumar, K. R.; Santra, A. K.; Rao, C. N. R. *Appl. Surf. Sci*. **1996**, *93*, 135.
(15) Burch, R.; Golunski, S. E.; Spencer, M. S. *Catal. Lett.* **1990**, *5*, 55.
(16) Spencer, M. S. *Catal. Lett.* **1998**, *50*, 37.
(17) Spencer, M. S. *Topics Catal*. **1999**, *8*, 259.
(18) Campbell, C. T. *Surf. Sci. Rep*. **1997**, *27*, 1.
(19) Barteau, M. A.; Vohs, J. M. *Stud. Surf. Sci. Catal*. **1989**, *44*, 89.
(20) Bowker, M.; Houghton, H.; Waugh, K. C.; Giddings, T.; Green, M. *J. Catal*. **1983**, *84*, 252.
(21) Grunze, M.; Hirschwald, W.; Hofmann, D. *Crystal Growth, J*. **1981**, *52*, 241.
(22) Diebold, U. *Surf. Sci. Rep*. **2003**, *48*, 53.
(23) Henry, C. R. *Surf. Sci. Rep*. 1098, *31*, 231.
(24) Dulub, O.; Boatner, L. A.; Diebold, U. *Surf. Sci*. **2002**, *504*, 271.
(25) Guo, Q.; Møller, P. J. *Appl. Surf. Sci*. **1997**, *115*, 39.
(26) Didziulis, S. V.; Butcher, K. D.; Cohen, S. L.; Solomon, E. I. *J. Am. Chem. Soc*. **1989**, *111*, 7110.
(27) Møller, P. J.; Nerlov, J. *Surf. Sci*. **1994**, *307*−*309*, 591.
(28) Yoshihara, J.; Campbell, J. M.; Campbell, C. T. *Surf. Sci*. **1998**, *406*, 235.
(29) Yoshihara, J.; Campbell, C. T. *Surf. Sci*. **1998**, *407*, 256.
(30) Yoshihara, J.; Parker, S. C.; Campbell, C. T. *Surf. Sci*. **1999**, *439*, 153.
(31) Jedrecy, N.; Gallini, S.; Sauvage-Simkin, M.; Pinchaux, R. *Phys. Rev. B: Condens. Matter Mater. Phys.* **2001**, *64*, 085424/1.
(32) Ludviksson, A.; Zhang, R.; Campbell, C. T.; Griffiths, K. *Surf. Sci*. **1994**, *313*, 64.
(33) Ludviksson, A.; Ernst, K. H.; Zhang, R.; Campbell, C. T. *J. Catal*. **1993**, *141*, 380.
(34) Zhang, R.; Ludviksson, A.; Campbell, C. T. *Surf. Sci*. **1993**, *289*, 1.
(35) Ernst, K. H.; Ludviksson, A.; Zhang, R.; Yoshihara, J.; Campbell, C. T. *Phys. Rev. B: Condens. Matter Mater. Phys.* **1993**, *47*, 13782.
(36) Vitos, L.; Ruban, A. V.; Skriver, H. L.; Kollar, J. *Surf. Sci*. **1998**, *411*, 186.
(37) Meyer, B.; Marx, D. *Phys. Rev. B: Condens. Matter Mater. Phys.* **2003**, *67*, 035403/1.
(38) Campbell, C. T.; Grant, A. W.; Starr, D. E.; Parker, S. C.; Bondzie, V. A. *Topics Catal*. **2001**, *14*, 43.
(39) Mariano, A. N.; Hanneman, R. E. *J. Appl. Phys*. **1963**, *34*, 384.
(40) Worren, T.; Højrup Hansen, K.; Laegsgaard, E.; Besenbacher, F.; Stensgaard, I. *Surf. Sci*. **2001**, *477*, 8.
(41) Cimino, A.; Mazzone, G.; Ports, P. *Z. Physik. Chem*. **1964**, *41*, 154.
(42) Dulub, O.; Boatner, L. A.; Diebold, U. *Surf. Sci*. **2002**, *519*, 201.
(43) Henrich, V. E.; Zeiger, H. J.; Solomon, E. I.; Gay, R. R. *Surf. Sci*. **1978**, *74*, 682.
(44) Dulub, O.; Diebold, U.; Kresse, G. *Phys. Rev. Lett.* **2003**, *90*, 016102/1.
(45) Wander, A.; Schedin, F.; Steadman, P.; Norris, A.; McGrath, R.; Turner, T. S.; Thornton, G.; Harrison, N. M. *Phys. Rev. Lett.* **2001**, *86*, 3811.
(46) Girard, R. T.; Tjernberg, O.; Chiaia, G.; Soederholm, S.; Karlsson, U. O.; Wigren, C.; Nylen, H.; Lindau, I. *Surf. Sci*. **1997**, *373*, 409.
(47) Göpel, W.; Pollmann, J.; Ivanov, I.; Reihl, B. *Phys. Rev. B: Condens. Matter Mater. Phys.* **1982**, *26*, 3144.
(48) Meyer, B. Los Alamos National Laboratory, Preprint Archive, Condensed Matter, 2003, 1.
(49) Kunat, M.; Girol, S. G.; Becker, T.; Burghaus, U.; Wöll, C. *Phys. Rev. B: Condens. Matter Mater. Phys.* **2002**, *66*, 081402.
(50) Staemmler, V.; Fink, K.; Meyer, B.; Marx, D.; Kunat, M.; Gil Girol, S.; Burghaus, U.; Wøll, C. *Phys. Rev. Lett*. **2003**, *90*, 106102/1.
(51) Ehrlich, G.; Hudda, F. G. *J. Chem. Phys*. **1966**, *44*, 039.
(52) Højrup Hansen, K.; Worren, T.; Stempel, S.; Lægsgaard, E.; Bäumer, M.; Freund, H. J.; Besenbacher, F.; Stensgaard, I. *Phys. Rev. Lett*. **1999**, *83*, 4120.
(53) Kaischew, R. *Bull. Acad. Sci. Ser. Phys*. **1951**, *2*, 191.
(54) Winterbottom, W. L. *Acta Metall.* **1967**, *15*, 303.
(55) Wulff, G. *Z. Kristallog.* **1901**, *34*, 449.
(56) Markov, I. V. *Crystal Growth for Beginners*; World Scientific: Singapore, 1995.
(57) Højrup Hansen, K. Ph.D. Thesis. Aarhus, 2001.
(58) Hansen, P. L.; Wagner, J. B.; Helveg, S.; Rostrup-Nielsen, J. R.; Clausen, B. S.; Topsoe, H. *Science* **2002**, *295*, 2053.
(59) Kallinteris, G. C.; Papanicolaou, N. I.; Evangelakis, G. A.; Papaconstantopoulos, D. A. *Phys. Rev. B: Condens. Matter Mater. Phys.* **1997**, *55*, 2150.
(60) Raouafi, F.; Barreteau, C.; Desjonqueres, M. C.; Spanjaard, D. *Surf. Sci*. **2002**, *505*, 183.
(61) Mattsson, A. E.; Jennison, D. R. *Surf. Sci*. **2002**, *520*, L611.
(62) Campbell, C. T.; Starr, D. E. *J. Am. Chem. Soc*. **2002**, *124*, 9212.
(63) Bogicevic, A.; Jennison, D. R. *Phys. Rev. Lett*. **1999**, *82*, 4050.
(64) Hume-Rothery, W.; Smallman, R. E.; Haworth, C. W. The Structure of Metals and Alloys, 5th ed.; *Institute of Metals Monograph and Report Series, No. 1*; 1969.
(65) Graoui, H. Giorgio, S.; Henry, C. R. *Philos. Mag*. **2001**, *81*, 1649.
(66) Graoui, H.; Giorgio, S.; Henry, C. R. *Surf. Sci*. **1998**, *417*, 350.
(67) Müller, P.; Kern, R. *Surf. Sci*. **2000**, *457*, 229.